Novel heterometal–organic complexes as first single source precursors for up-converting NaY(Ln)F–4 (Ln = Yb, Er, Tm) nanomaterials

ARTICLE *in* DALTON TRANSACTIONS · DECEMBER 2011

Impact Factor: 4.2 · DOI: 10.1039/c1dt11070e · Source: PubMed

5 AUTHORS, INCLUDING:

Shashank Mishra
Claude Bernard University Lyon 1
68 PUBLICATIONS **438** CITATIONS
SEE PROFILE

G. Ledoux
Claude Bernard University Lyon 1
129 PUBLICATIONS **2,578** CITATIONS
SEE PROFILE

Erwann Jeanneau
Claude Bernard University Lyon 1
188 PUBLICATIONS **1,394** CITATIONS
SEE PROFILE

Stephane Daniele
French National Centre for Scientific Resea…
150 PUBLICATIONS **1,184** CITATIONS
SEE PROFILE

Dalton Transactions

Cite this: *Dalton Trans.*, 2012, **41**, 1490

www.rsc.org/dalton

PAPER

Novel heterometal-organic complexes as first single source precursors for up-converting $NaY(Ln)F_4$ (Ln = Yb, Er, Tm) nanomaterials†

Shashank Mishra,*[a,b] Gilles Ledoux,[b] Erwann Jeanneau,[c] Stéphane Daniele*[a] and Marie-France Joubert*[b]

Received 7th June 2011, Accepted 13th October 2011
DOI: 10.1039/c1dt11070e

First heterometal–organic single source precursors for $NaYF_4$ nanomaterials as a host matrix for up-conversion emission are reported. These novel heterobimetallic derivatives $NaY(TFA)_4$(diglyme) (**1**), $[Na(triglyme)_2][Y_2(TFA)_7(THF)_2]$ (**2**) and $Na_2Y(TFA)_5$(tetraglyme) (**3**) (TFA = trifluoroacetate), which were fully characterized by elemental analysis, FT-IR and ^{1}H NMR spectroscopy, TG-DTA data as well as single crystal X-ray structures, are advantageous in terms of being anhydrous and having lower decomposition temperatures in comparison to the homometallic precursor $Y(TFA)_3(H_2O)_3$. In addition, they also contain chelating glyme ligands, which act as capping reagents during decomposition to control the $NaYF_4$ particle size and render them monodisperse in organic solvents. On decomposition in 1-octadecene, the molecular derivatives **1** and **3** are converted, in the absence of any surfactant or capping reagent, to cubic $NaYF_4$ nanocrystals at significantly lower temperatures (below 250 °C). At higher temperature, a mixture of the cubic and hexagonal phases was obtained, the relative ratio of the two phases depending on the reaction temperature. A pure hexagonal phase, which is many folds more efficient for UC emission than the cubic phase, was obtained by calcining nanocrystals of mixed phase at 400 °C. In order to co-dope this host matrix with up-converting lanthanide cations, analogous complexes $NaLn(TFA)_4$(diglyme) [Ln = Er (**4**), Tm (**5**), Yb (**6**)] and $Na_2Ln(TFA)_5$(tetraglyme) [Ln = Er (**7**), Yb (**8**)] were also prepared and characterized. The decomposition in 1-octadecene of suitable combinations and appropriate molar ratios of these yttrium, ytterbium and erbium/thulium derivatives gave cubic and/or hexagonal $NaYF_4$: Yb^{3+}, Er^{3+}/Tm^{3+} nanocrystals (NCs) capped by diglyme or tetraglyme ligands, which were characterized by IR, TG-DTA data, EDX analysis and TEM studies. Surface modification of these NCs by ligand exchange reactions with poly acrylic acid (PAA) and polyethyleneglycol (PEG) diacid 600 was also carried out to render them water soluble. The THF solutions of suitable combinations of the diglyme derivatives were also used to elaborate the thin films of $NaYF_4$:Yb^{3+}, Er^{3+}/Tm^{3+} on a glass or Si wafer substrate by spin coating. The multicolour up-conversion fluorescence was successfully realized in the Yb^{3+}/Er^{3+} (green/red) and Yb^{3+}/Tm^{3+} (blue/violet) co-doped $NaYF_4$ nanoparticles and thin films, which demonstrates that they are promising UC nanophosphors of immense practical interest. The up-conversion excitation pathways for the Er^{3+}/Yb^{3+} and Tm^{3+}/Yb^{3+} co-doped materials are discussed.

Introduction

Lanthanide-doped up-conversion (UC) emission materials, which convert near-infrared (NIR) light to visible light by a non-linear multi-photon absorption process, have attracted tremendous interest due to their potential use as luminescent macro- or nano-devices ranging from solid state lasers and optical data storage to next generation lighting or display.[1–3] In particular, the nanoscale UC materials have emerged as promising next generation alternatives to organic dyes and quantum dots for applications in the field of biological assay and medical imaging.[4] Unlike organic fluorophores and quantum dots, the use of UC nanomaterials offers low autofluorescence (background noise), sharp emission bandwidths, high quantum yields, long life times, high resistance to photobleaching, high penetration depth and minimum photo damage to biological specimen.[5] Among various

[a]*University of Lyon 1, IRCELYON, 2 Avenue A. Einstein, 69626, Villeurbanne, France. E-mail: mishrashashank74@rediffmail.com; Fax: 33 472445399; Tel: 33 472445329*
[b]*University of Lyon 1, Laboratoire de Physico Chimie des Matériaux Luminescent, 10 rue A. M. Ampére, 69622, Villeurbanne, France*
[c]*University of Lyon 1, Centre de Diffractométrie, 69622, Villeurbanne, France*

† Electronic supplementary information (ESI) available: FT-IR spectra of **1–8**, ^{1}H NMR spectra of diamagnetic **1–3**, TG-DTA curves for the $NaYF_4$: Yb^{3+}, Er^{3+}/Tm^{3+} NCs obtained at different temperature, EDX analyses of the thin films, solution- and solid-phase emission spectra of $NaYF_4$: Yb^{3+}, Er^{3+}/Tm^{3+} NCs showing effect of ageing, NCs, additional figures showing the intensity of the difference bands of up-converting NCs with the excitation power. Two X-ray crystallographic files in CIF format. CCDC reference numbers 796485 and 796486 for **2** and **3**, respectively. For ESI and crystallographic data in CIF or other electronic format see DOI: 10.1039/c1dt11070e

host materials for UC emission, $NaYF_4$ is most promising and hence has garnered much attention.[2,3,6] This material exists in two polymorphic forms at ambient pressure and temperature: the cubic (α) and the hexagonal (β), the latter phase being the most efficient host matrix for UC emission.[7] Since 1972, when Menyuk *et al.* first reported superiority of the above material over YF_3 for NIR-to-visible conversion,[8] several methods have been developed to obtain bulk $NaYF_4$.[3,6] However, it was not until the beginning of this century when $NaYF_4$ crystals (doped and co-doped with up-converting lanthanide cations) could be obtained in the nanoscale using wet chemical methods. An early example was provided by Haase and co-workers who obtained cubic-phase $NaYF_4$:Yb^{3+}, Er^{3+}/Tm^{3+} NCs using methanol as the organic solvent.[9] In the same year, Yi *et al.* reported a co-precipitation method using $LnCl_3$, NaF and ethylene diamine tetraacetic acid (EDTA) in aqueous medium, followed by calcinations of the obtained powder up to 600 °C to get hexagonal $NaYF_4$: Yb^{3+}, Er^{3+} NCs.[10] Different groups have also reported the synthesis of lanthanide co-doped hexagonal $NaYF_4$ nano-crystals, -rods and -disks of variable size by hydro- and solvo-thermal methods.[11] Then Chen *et al.* used metal oleate and NaF to synthesize β-$NaYF_4$ nanoplates with a liquid/solid heterogeneous reaction.[12] The nucleation and growth process was localized at the two-phase interface, and an interface transfer mechanism was proposed to explain the narrow size distribution of NCs. Li's group applied a more complicated three-phase liquid-solid-solution (LSS) procedure involving ethanol–aliphatic acid (liquid)-metal aliphatate salt (solid)-water/ethanol (solution) phases to prepare uniform α- and β-phase $NaYF_4$ NCs.[13] More recently, an ionothermal[14] and a microwave-assisted[15] synthesis of these up-converting nanomaterials have also appeared.

However, the above methods suffered from different drawbacks ranging from unfriendly experimental conditions, such as dealing with highly corrosive and toxic reagents, high reaction temperature, requirement of specialized reaction vessels, *etc*, to undesired forms of materials like large particle size, getting cubic phase alone and particle aggregation. A soft chemical approach or '*Chimie douce*' is an alternate route to solid-state materials where a molecular compound containing the component element(s) is used in a chemical vapor deposition (CVD), Metal–Organic Decomposition (MOD) or sol–gel process to obtain high-purity films or powders.[16] These chemical routes overcome many of the drawbacks of the physical methods listed above and facilitate a better control over the composition, structure and morphology of the nanomaterials.[16] Except for co-thermolysis of lanthanide trifluoroacetate precursors,[17] the above methods have rarely been explored for the synthesis of $NaYF_4$ materials and the prime reason for it is the unavailability of suitable metallic precursors. High-quality α- and/or β-phase $NaYF_4$:Yb, Er(Tm) NCs were prepared using CF_3COONa and $Ln(CF_3COO)_3(H_2O)_x$ in the presence of various coordinating ligands to control the sizes of NCs with high up-conversion luminescence.[17] The selection of a proper coordinating ligand [oleic acid (OA), oleyl amine (OM), trioctylphosphine (TOP), trioctylphosphine oxide (TOPO)] or ligand combinations such as OA-TOP controls the $NaYF_4$ synthesis by dictating the particle nucleation and growth and is one of the key factors for achieving monodisperse and size-tunable colloidal NCs. In this context, we were interested in a one-step synthesis of $NaY(Ln)F_4$ materials using single source heterometallic precursors containing all the required elements (Na, Y/Ln, F) in a single molecule, which would not only ensure greater homogeneity at atomic levels and the absence of unnecessary contaminating ions but also make it easy to control the process.

In a preliminary communication,[18] we recently reported heterometallic [$NaLn(TFA)_4$(diglyme)] as the first single source precursor for the formation of $NaY(Ln)F_4$ nanocrystals. We describe here a complete study on the synthesis and characterization of a series of heterometallic Na-Y(Ln) trifluoroacetate complexes with glyme ligands and the inherent advantages of using these rationally designed complexes as single-source precursors to obtain the lanthanide-doped $NaY(Ln)F_4$ nanocrystals and thin films under mild conditions for the up-converting process. These heterometallic complexes are not only the first single source precursors for up-converting $NaY(Ln)F_4$ materials but also represent rare class of metal–organic precursors for any other heterometal fluoride nanomaterials in general. To the best of our knowledge, the very recently reported $PbM(hfac)_4$ (M = Ni, Co, Mn, Fe, Zn; hfac = hexafluoroacetylacetonate) are the only other known SSPs for such materials.[19] The complexes reported here have multiple advantages over the homometallic $Ln(TFA)_3(H_2O)_3$, which were used recently as precursors for up-converting $NaYF_4$:Ln^{3+} nanomaterials.[17] First, the synthetic procedure used is a simple one that affords almost quantitative yield of anhydrous heterometallic molecules. Formation of anhydrous heterometallic derivatives is particularly significant as the presence of water molecules is detrimental for the up-converting properties of $NaY(Ln)F_4$ NCs. The cost-efficient synthesis of lanthanide trifluoroacetate by reacting Ln_2O_3 with trifluoroacetic acid in refluxing toluene proceeds with the formation of water as a by-product to afford the hydrated complex $Ln(TFA)_3(H_2O)_3$. However, efforts to get rid of water molecules in $Y(TFA)_3(H_2O)_3$, either by thermal dehydration or ligand exchange reactions, have proven difficult.[20] Second, the decomposition temperature of these Na-Y heterometallics is considerably lower than that of homometallic precursor. Third, the molecular precursor derivatives with diglyme or tetraglyme ligand have either 1 : 1 or 2 : 1 stoichiometry of the Na and Ln metals, respectively, which on decomposition give the desired $NaY(Ln)F_4$ material (the additional NaF phase formed during the decomposition of tetraglyme precursors can easily be washed out by water). Last but not the least, unlike conventional strategies, no additional capping-reagents or surfactants were needed in this work to control the size of the $NaY(Ln)F_4$ nanocrystals and render them monodisperse in organic media, as the glyme ligand present in the coordination sphere of heterometallics acts as one during decomposition. The hydrophobic glyme ligand on the surface of as-prepared NCs can easily be exchanged with hydrophilic ligands such as polyacrylic acid and polyethylene glycol diacid 600. This imparts water solubility to the as-prepared NCs and also affords some functional groups on their surfaces, facilitating conjugation of these NCs with biomolecules for potential bio-applications. In addition, the solutions of these precursors in organic solvents are amenable to spin/dip coating for the elaboration of thin films on a substrate of desired shape.

Results and discussion

(a) Synthesis and spectroscopic properties

Equivalent reactions of $Y(TFA)_3(H_2O)_3$ and NaTFA (TFA = trifluoroacetate anion) in THF in the presence

of di-, tri-, and tetraglyme proceed smoothly to give anhydrous heterometallic derivatives $YNa(TFA)_4$(diglyme) (**1**), $[Na(triglyme)_2][Y_2(TFA)_7(THF)_2]$ (**2**) and $Na_2Y(TFA)_5$-(tetraglyme) (**3**), respectively, in a good to excellent yield. The derivatives **2** and **3**, which have 1 : 2 and 2 : 1 ratios of sodium and yttrium metals, respectively, can be obtained in better yields if stoichiometric amounts of sodium and yttrium reagents corresponding to their respective formula are employed. Unlike complex **2**, which is an ion pair of an triglyme-wrapped discrete sodium cation and 1D yttrium trifluoroacetate anionic chain, the **1** and **3** are neutral molecular complexes and hence were chosen as single source precursors for $NaYF_4$ materials. In order to co-dope this $NaYF_4$ host matrix with up-converting ytterbium and erbium/thulium cations, analogous lanthanide complexes $NaLn(TFA)_4$(diglyme) [Ln = Er (**4**), Tm (**5**), Yb (**6**)] and $Na_2Ln(TFA)_5$(tetraglyme) [Ln = Er (**7**), Yb (**8**)] were also prepared. Compounds **1–8** are soluble in THF and CH_3CN but insoluble in n-hexane and diethyl ether. The formation of heterometallic derivatives **1–8** assumes great significance as these anhydrous derivatives not only ensure the complete absence of water during decomposition experiments as well as lowering the decomposition temperature [compared to $Ln(TFA)_3(H_2O)_3$], but also deliver the glyme ligand as a capping reagent to control the size of $NaY(Ln)F_4$ NCs and render them mono-disperse in organic solvents.

The FT-IR spectra of **1–8** account for the anhydrous species (Fig. S1†). These spectra, which are dominated by strong absorptions in the carbonyl region 1350–1760 cm^{-1}, indicate that the trifluoroacetate ligand is in different bonding modes. Usually the $\nu_{as}CO_2$ stretching frequencies for the purely bridging TFA are observed at higher wave numbers than those concerned with either chelating or both bridging and chelating TFA.[21] Besides, the number and type of donating atoms of the coordinating ligand on the metal center also affects the position of this frequency.[22] Whereas two medium to strong intensity bands for $\nu_{as}CO_2$ stretching are observed in the region 1759–1785 and 1680–1683 cm^{-1} for diglyme complexes **1** and **4–6**, suggesting at least two different environments of TFA ligand, an overlapping of the same absorption due to three different bonding modes of the TFA ligands results in a strong broad band centered around 1680 cm^{-1} in tetraglyme complexes **3**, **7** and **8**. Strong C–F and C–O absorption bands in the 1120–1210 cm^{-1} range, three characteristic TFA absorptions in the 850–720 cm^{-1} region and the low frequency absorptions at 632–404 cm^{-1} due to the ν Ln–O vibration also characterized the spectra of **1–8**.[23] Compared to IR spectra, the ^1H NMR spectra of the diamagnetic **1–3** are structurally less diagnostic. These spectra, however, do indicate single environments for glyme ligands in these derivatives by showing only one set of protons for glyme ligands (Fig. S2†). The coordinated THF molecules in **2** appear as two triplets in the expected integral ratio at δ 1.81–1.89 (β-H) and 3.66–3.70 (α-H) ppm for and hydrogens, respectively. The spectrum of **3** shows a 4 : 1 integral ratio of the tetraglyme ligand and the solvated diethyl ether molecule, appearing as a triplet and a quartet at δ 1.1 and 3.3 ppm, respectively, which is consistent with the observation made in experimental section that half of the diethyl ether molecules are lost under vacuum while drying the product.

(b) Single crystal X-ray structures of 1–3

The identity of the yttrium complexes **1–3** was further established by single crystal X-ray diffraction study. The structure of $[Y(\mu\text{-}\eta^1\text{:}\eta^1\text{-TFA})_2(\mu_3\text{-}\eta^2\text{(O,F)}\text{:}\eta^1\text{:}\eta^1\text{-TFA})_2Na(\eta^3\text{-diglyme})]_{1\infty}$ (**1**) can be described as the 1D polymeric Y-TFA chain containing doubly- and triply-bridging TFA ligands, the latter also connecting peripheral $[Na(\eta^3$-diglyme)] units *via* one O and one F centers (Fig. 1).[18] The eight-coordinated yttrium centers exhibit a rather regular square antiprismatic geometry.[24] The peripheral sodium atoms are 7-coordinate, each being connected with three oxygen atoms of a diglyme as well as one oxygen and one fluorine atoms each of two triply bridging TFA moieties. The Y–O and Na–O bond distances spread over the range, 2.301(5)–2.427(4) Å and 2.326(7)–2.423(6) Å, respectively, the average distance for the latter involving bridging TFA ligands (2.358 Å) being slightly shorter than the ones involving chelating diglyme ligand (av. 2.380 Å).

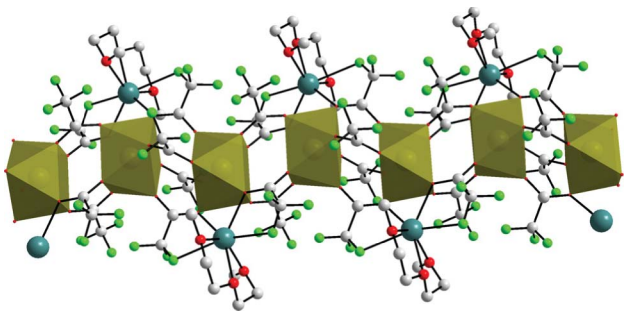

Fig. 1 One-dimensional structure of **1**. H-atoms on diglyme ligands have been omitted for clarity. Color scheme same as shown in Fig. 2.

The ionic **2** consists of 1D-polymeric chain of the composition $[Y_2(\mu\text{-}\eta^1\text{:}\eta^1\text{-TFA})_7(THF)_2]^-$, which runs along the *c*-axis of the unit cell.‡. The charge for above unit is balanced by a discrete $[Na(\eta^4$-triglyme$)_2]^+$ cation (Fig. 2). The yttrium centres are bridged by four and three $\eta^1\text{:}\eta^1$-trifluoroacetate ligands in an alternate manner (Fig. 2). A tetrahydrofuran (THF) molecule on each yttrium centre ensures 8-coordination number and a bicapped trigonal prismatic geometry around the metal.[24] The Y–O (TFA) bond distances, which range from 2.275(9) to 2.342(9) Å, are in agreement with the body of literature on 8-coordinated yttrium complexes.[22,23] On the other hand, the Y–O (THF) bond distance, 2.504(8) Å, is slightly longer than the values (av. 2.43 Å) found in some other yttrium-THF adducts,[25] indicating a relatively weakly coordinated THF in **2**. The Y···Y distance, 4.602(8) Å, is slightly shorter when they are bridged by four TFA ligands in comparison to that of 4.985(8) Å, when only three TFA act as bridges. The sodium ion

‡ Crystal structure data for (**2**): $C_{38}H_{52}F_{21}NaO_{24}Y_2$, M_r = 1492.61, Orthorhombic, *Pcca*, a = 29.260(4) Å, b = 11.863(1) Å, c = 18.725(2) Å, V = 6499.7(13) Å^3, Z = 4, μ = 1.91 mm^{-1}, T = 180 K, 7725 measured reflections, 7725 independent reflections, R_{int} = 0.095, $R[F^2 > 2\sigma(F^2)]$ = 0.082, $wR(F^2)$ = 0.186, S = 1.23, reflections/restrains/parameters 7725/141/457, $\Delta\rho_{max}$ = 2.43 e Å^{-3}, $\Delta\rho_{min}$ = −2.29 e Å^{-3}. (**3**): $C_{44}H_{54}F_{30}Na_4O_{31}Y_2$, M_r = 1918.60, Orthorhombic, $P2_1cn$ (a non-standard setting of $Pna2_1$), a = 17.8642(3) Å, b = 19.6674(4) Å, c = 21.2130(4) Å, V = 7453.0(2) Å^3, Z = 4, μ = 1.73 mm^{-1}, T = 150 K, 16664 measured reflections, 16181 independent reflections, R_{int} = 0.074, $R[F^2 > 2\sigma(F^2)]$ = 0.067, $wR(F^2)$ = 0.180, S = 0.95, reflections/restrains/parameters 16167/38/1001, $\Delta\rho_{max}$ = 1.32 e Å^{-3}, $\Delta\rho_{min}$ = −1.02 e Å^{-3}, Flack parameter = 0.472(7).

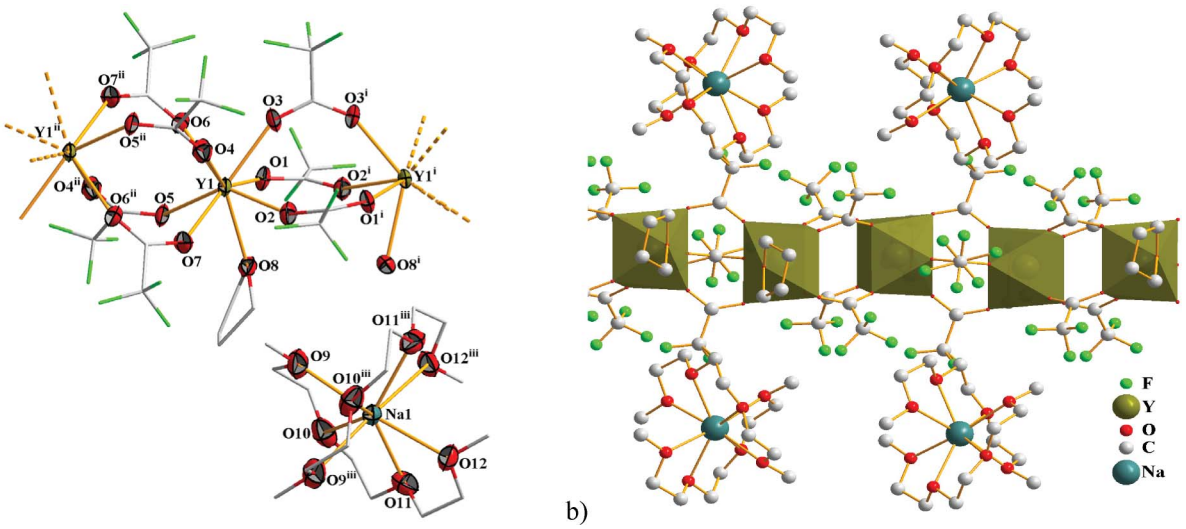

Fig. 2 X-ray structure of **2**: a) ORTEP with ellipsoid at 30% probability (H-atoms are omitted for clarity); b) 1D chain along *c* axis. Selected bond lengths (Å) and angles (°): Y1–O2 2.275(9), Y1–O8 2.504(8), Na1–O9 2.529(13), Na1–O10 2.619(12), O1–Y1–O8 71.6(3), O2–Y1–O4 82.7(3), O3–Y1–O7 140.0(4), O11–Na1–O12 62.8(4), O9^{iii}–Na1–O12 93.9(4), O10^{iii}–Na1–O10 137.3(6). Symmetry codes: (i) $-x + 1, y, -z + 3/2$; (ii) $-x + 1, -y + 1, -z + 1$; (iii) $-x + 1/2, -y, z$.

in the $[Na(\eta^4\text{-triglyme})_2]^+$ cation is coordinated by eight oxygen atoms of two triglyme ligands. The four oxygen atoms of each triglyme ligand lie approximately in a plane and the planes of the two triglyme ligands are perpendicular to each other leading to a somewhat regular dodecahedral geometry for the sodium ion.[24] Similar wrapping by two glyme ligands in a perpendicular manner has been previously reported for some of the alkali and alkaline earth metal cations.[26] The Na–O (triglyme) bond lengths range from 2.529(13)–2.619(12) Å, the average distance (2.59 Å) being slightly longer than the Na–O (diglyme) distance in **1** (av. 2.37 Å) due to the higher coordination number and the ionic character of sodium centre in **2**.[26] It should be noted that the sodium atom Na1 lies on a twofold axis parallel to the *c* axis of the unit-cell whereas the carbon atoms C3 and C4 lie on another twofold axis along the *b* axis of the unit-cell.

The structure of **3** is composed of the repetitive $[Y_2Na_4(\mu\text{-}\eta^1\text{:}\eta^1\text{-TFA})_4(\mu_3\text{-}\eta^1\text{:}\eta^2(O,O)\text{:}\eta^1\text{-TFA})_2(\mu_3\text{-}\eta^2(F,O)\text{:}\eta^1\text{:}\eta^1\text{-TFA})_2(\mu_3\text{-}\eta^1\text{:}\eta^1\text{:}\eta^1\text{-TFA})_2Na(\mu\text{-}\eta^5\text{:}\eta^1\text{-tetraglyme})_2]$ units, each unit being associated with other such units *via* three $\mu\text{-}\eta^1\text{:}\eta^1$-TFA groups, thus giving rise a 1D polymeric chain along the *c* direction of the unit cell (Fig. 3). The formation of above hexanuclear Y_2Na_4 building block is facilitated by six triply bridging TFA ligands, acting in three different $\eta^2(F,O)\text{:}\eta^1\text{:}\eta^1$, $\eta^1\text{:}\eta^2(O,O)\text{:}\eta^1$ and $\eta^1\text{:}\eta^1\text{:}\eta^1$ manners, which ensure the connectivity between the yttrium and sodium centers. Two doubly bridging ligands, a $\eta^1\text{:}\eta^1$-TFA between two yttrium atoms and a $\eta^5\text{:}\eta^1$-tetraglyme between two sodium atoms, further consolidate this assembly. Each yttrium center is coordinated to seven oxygen atoms, one each from four doubly bridging and three triply bridging TFA ligands, with the Y–O distances spreading in the range 2.241(6)–2.347(5) Å. A rare secondary F···Y bond [2.955(5)–3.012(6) Å] then completes the 8-coordination number around each yttrium center, which is the usual coordination number observed previously in yttrium trifluoroacetate complexes.[20,22] The sodium metal centers, on the other hand, have two different coordination environments. The most peripheral sodium atoms are 7-coordinate, bound by five oxygen atoms of a tetraglyme ligand and one oxygen each from the triply bridging $\eta^2(F,O)\text{:}\eta^1\text{:}\eta^1$ and $\eta^1\text{:}\eta^2(O,O)\text{:}\eta^1$ TFA ligands, and have a distorted pentagonal bipyramidal geometry. In contrast, a somewhat distorted octahedral geometry around the two sodium centers closer to the Y-TFA chain is achieved by two O atoms of a $\mu_3\text{-}\eta^1\text{:}\eta^2(O,O)\text{:}\eta^1$–TFA ligand and one O each of a $\mu_3\text{-}\eta^2(F,O)\text{:}\eta^1\text{:}\eta^1$–TFA, two $\mu_3\text{-}\eta^1\text{:}\eta^1\text{:}\eta^1$–TFA and a $\mu\text{-}\eta^5\text{:}\eta^1$-tetraglyme ligand. The bridging $\eta^5\text{:}\eta^1$ coordination mode of tetraglyme ligand has previously been observed in $[Ba_2(TFA)_4(tetraglyme)]$.[27] The Na–O bond distances spread over the range 2.334(6)–2.694(6) Å and 2.314(5)–2.755(6) Å for 7- and 6-coordinated sodium centers, respectively. The Y···Y distance within the Y_2Na_4 assembly [5.4648(8) Å] is longer than the one found between yttrium centres of two Y_2Na_4 units bridged by three TFA ligands [5.1936(8) Å]. These distances are also considerably longer than those found in **1** [av. 4.530 Å].

There are two unique features among the crystal structures reported here, which require further comments: i) the rare secondary F···M bonds in **1** [F23···Na1 2.695(6) Å, F16···Na2 2.655(6) Å] and **3** [F21···Y1 2.955(5) Å, F1···Y2 3.012(6) Å]. To the best of our knowledge, except for one barium complex,[22] there is no other precedence available of F···M interactions involving a trifluoroacetate ligand, even though such an interaction is a common feature for metal derivatives of fluorinated alkoxide or β-diketonate ligands,[28] and ii) two new triply bridging coordination modes of the TFA ligand, namely $\mu_3\text{-}\eta^1\text{:}\eta^1\text{:}\eta^1$ and $\mu_3\text{-}\eta^2(O,F)\text{:}\eta^1\text{:}\eta^1$, which are reported here for the first time. The previously known triply bridging coordination modes of the TFA ligand are $\mu_3\text{-}\eta^1\text{:}\eta^2(O,O')\text{:}\eta^1$ and $\mu_3\text{-}\eta^2(O,O')\text{:}\eta^2(O,F)\text{:}\eta^1$.[22]

(c) Thermo-gravimetric studies

The thermal behavior of heterometallic Na-Y derivatives **1–3** was investigated by thermogravimetry (TG) and differential thermal

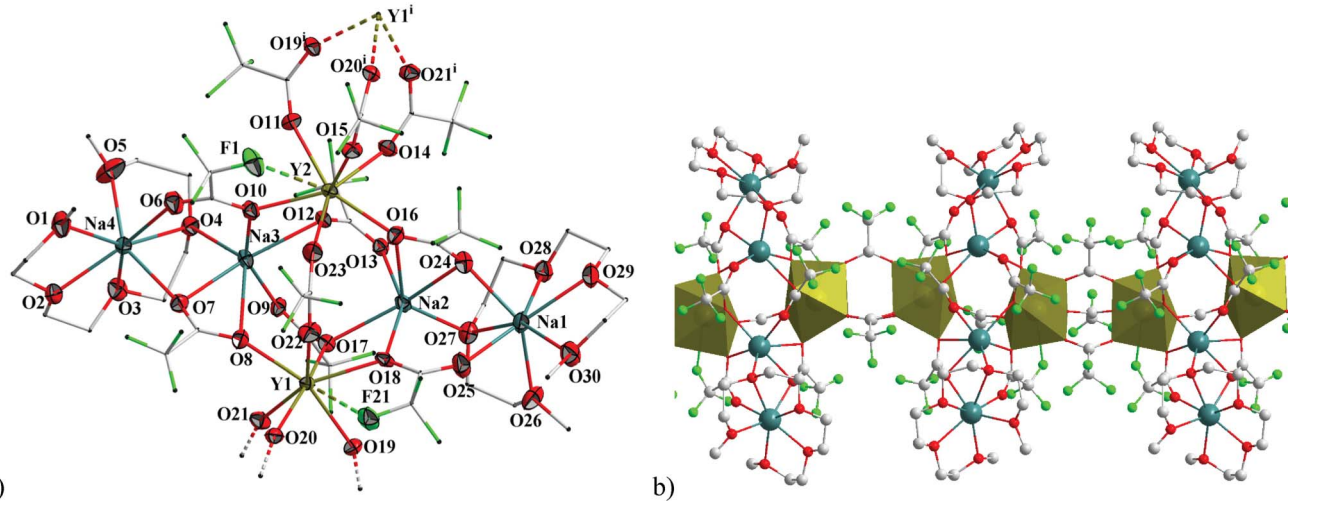

Fig. 3 X-ray structure of **3**: a) ORTEP with ellipsoid at 30% probability. For clarity, H-atoms are omitted and C and F atoms are drawn as ball and stick (except those involved in F–M interactions); b) 1D chain along *c* axis. Colour scheme same as shown in Fig. 2. Selected bond lengths (Å) and angles (°): O20–Y1 2.241(6), O18–Y1 2.332(4), O15–Y2 2.231(5), O10–Y2 2.347(4), O24–Na1 2.374(6), O13–Na2 2.314(5), O16–Na2 2.755(6), F21 ··· Y1 2.955(5), Y2 ··· Na3 3.779(3), O18–Y1–O19 72.8(2), O18–Y1 ··· F21 57.8(2), F21 ··· Y1–O8 134.9(2), O29–Na1–O28 67.5(2), O30–Na1–O27 153.0(3). Symmetry codes: (i) $x, -y + 1/2, z - 1/2$; (ii) $x, -y + 1/2, z + 1/2$.

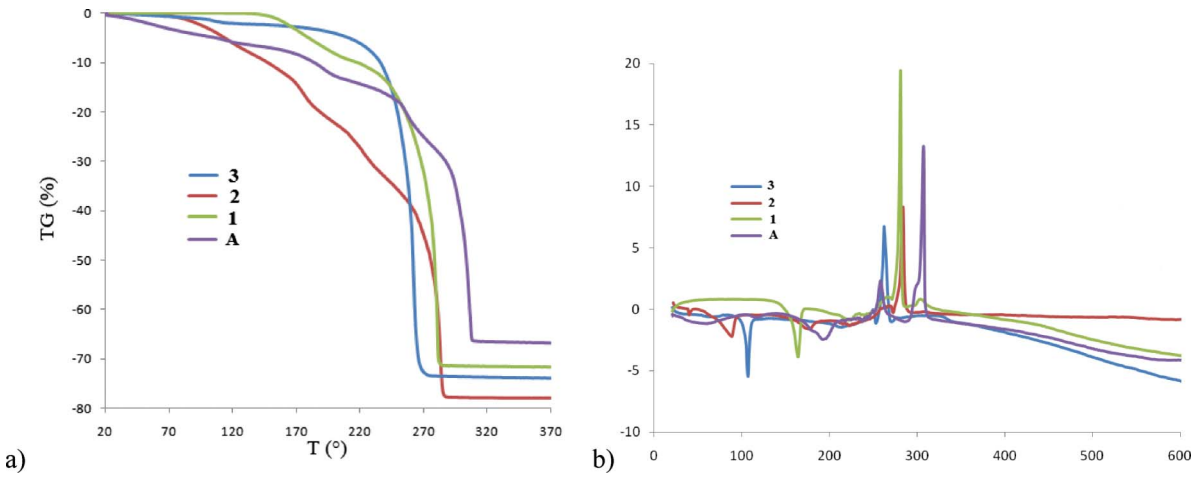

Fig. 4 TGA and DTA curves of **1–3** and $Y(TFA)_3(H_2O)_3$ (**A**).

analysis (DTA) under an argon atmosphere in the 20–650 °C temperature range (Fig. 4). For the sake of comparison, similar data were collected for the homometallic derivative $Y(TFA)_3(H_2O)_3$ (**A**) also. These data underline that the final decomposition temperature for the heterometallic Na-Y derivatives **1–3** (265–285 °C) is considerably lower than that found for the homometallic derivative (**A**) (310 °C), the precise order of the decomposition temperature being **3** < **2** ~ **1** < **A**. The multistep TG curves for **1–3** show that, after the removal of solvate molecules (Et_2O or THF) in the first few small steps, the major weight loss corresponding to thermal decomposition of the TFA and glyme ligands occurs in a single step, as indicated by a prominent exothermic peak at 280.5, 281.3 and 261.7 °C for **1–3**, respectively. The remaining weight of the residues 29.89, 23.4 and 27.4% for **1**, **2** and **3**, respectively, account a little more than the expected yield of $NaYF_4$ materials in **1** (26.92%), $NaYF_4$ + YF_3 in **2** (22.37%) and $NaYF_4$ + NaF in **3** (23.98%), indicating incomplete decomposition due to the presence of argon atmosphere.

(d) Preparation and characterization of $NaYF_4$:Yb^{3+}, Er^{3+}/Tm^{3+} nanocrystals

The molecular derivatives **1** and **3** start to decompose in 1-octadecene at 250 and 235 °C, respectively, to give only cubic $NaYF_4$ nanocrystals. The above temperature is significantly lower than the one at which homometallic $Y(TFA)_3(H_2O)_3$ (**A**) decomposes (see Fig. 4). Moreover, due to the presence of di- or tetraglyme ligands present in the coordination sphere of **1** and **3**, no additional capping-reagents or surfactants were needed to control the size of these $NaYF_4$ NCs and render them monodisperse in organic media. At higher temperature, a mixture of the cubic and hexagonal phases was obtained, where the relative ratio of the two phases depended on the reaction temperature. To obtain $NaYF_4$ NCs co-doped with 20% Yb^{3+} and 2% Er^{3+}/Tm^{3+} cations, the suitable combinations of derivatives (**1** + **4** + **6**, **1** + **5** + **6** or **3** + **7** + **8**) in appropriate amounts were decomposed simultaneously in 1-octadecene. The characterization of these $NaYF_4$:20% Yb^{3+},

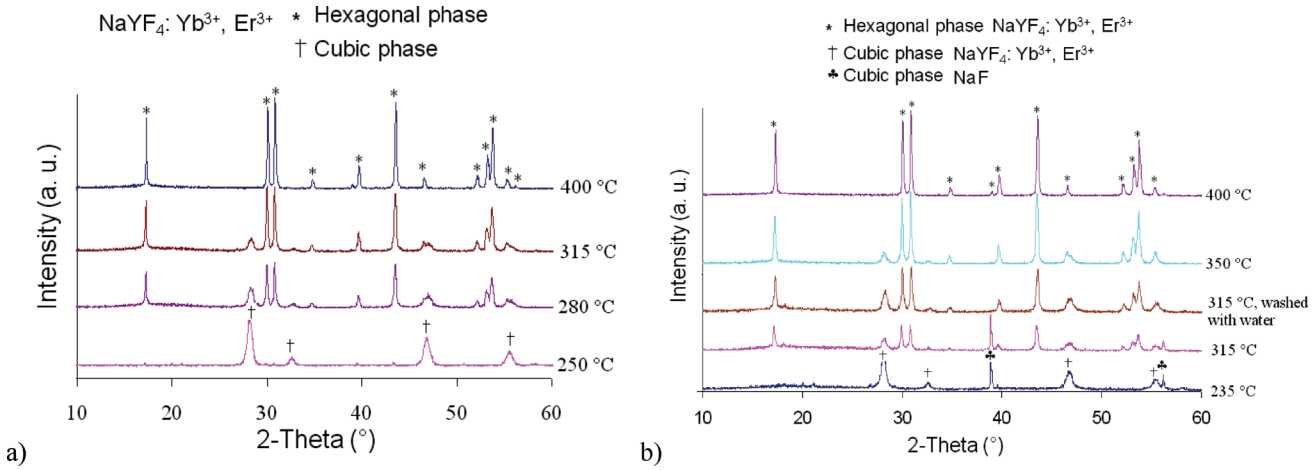

Fig. 5 Variable temperature XRD patterns of the $NaYF_4$: Yb^{3+}, Er^{3+}/Tm^{3+} NCs obtained from diglyme (a) and tetraglyme precursors (b).

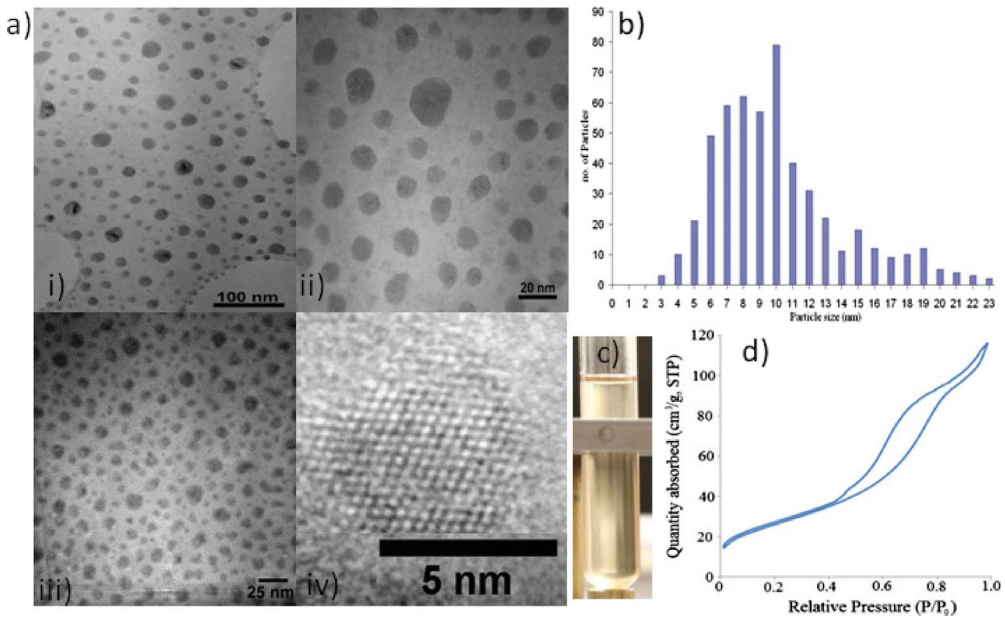

Fig. 6 a) TEM images of $NaYF_4$: Yb^{3+}, Er^{3+}/Tm^{3+} NCs: i) & ii) $NaYF_4$: Yb^{3+}, Tm^{3+} NCs obtained from diglyme precursors at 290 °C, iii) $NaYF_4$: Yb^{3+}, Er^{3+} NCs obtained from tetraglyme precursors and calcined at 350 °C, and iv) a high resolution TEM image; b) nanoparticle size distribution; c) a digital photograph of well-dispersed as-prepared NCs in CH_2Cl_2 and d) the nitrogen adsorption–desorption isotherms of cubic $NaYF_4$ NCs.

2% Er^{3+}/Tm^{3+} nanoparticles is summarized in Fig. 5 and 6. The variable temperature XRD patterns of the samples obtained from diglyme and tetraglyme complexes are shown in Fig. 5a and 5b, respectively. The NCs obtained below or at 250 °C are mainly in cubic phase (JCPDS: 077-2042). At higher temperature, the hexagonal phase also appears. As the reaction temperature increases, the relative ratio of the hexagonal phase increases and the NCs obtained at the boiling point of 1-octadecene (315 °C) show hexagonal phase as the major phase (JCPDS: 16-0334). A pure hexagonal phase, which is many folds more efficient for UC emission than the cubic phase, is obtained by calcinations of the mixed-phase NCs at 400 °C. Except for the fact that tetraglyme complexes start decomposing at a lower temperature (235 °C against 250 °C for diglyme complexes), the above pattern of decomposition is similar for complexes **1** and **3–8**. It was previously reported that presence of excess of NaTFA prompted the formation of hexagonal phase at relatively low temperature by disturbing the Ostwald ripening process.[29] However, we did not observe any such effect during the decomposition of tetraglyme complexes **3**, **7** and **8**, which have a 2 : 1 ratio of the sodium and yttrium/lanthanide metals. As expected, an additional phase of NaF was formed during the decomposition of above complexes, which could easily be got rid of by washing the NCs with water twice. Owing to the presence of glyme ligand on the surface, as confirmed by IR spectra and TG-DTA studies (Fig. S3†), these nanocrystals could be dispersed in solvents such as C_7H_8, CH_2Cl_2 and DMSO. The transmission electron microscopy (TEM) images show crystalline particles of nanometric size (Fig. 6a). A histrogram of the particle size distribution, as obtained by direct observation on TEM bright field images, is given in Fig. 6b, which shows a rather narrow size distribution in the range 3 to 23 nm. A mean particle size of 10.9 ± 4.6 nm, determined from the above

TEM data, is in good agreement with the average particle size calculated from the peak widths in XRD by using the Debye–Scherrer formula. The high resolution TEM image of a single particle clearly shows lattice fringes indicating high crystallinity of these particles. This analysis also confirms the single crystal nature of the product (Fig. 6).

The nitrogen adsorption–desorption isotherm of the NCs obtained at 250 °C (*i.e.* cubic phase) is shown in Fig. 6d. The observed hysteresis loop for this sample exhibits the shape that is characteristic for mesoporous materials. BET surface area and BJH average pore diameter were found to be 95.9 m^2 g^{-1} and 6.1 nm, respectively. Obviously, the high surface area and the porosity observed here are due to the surface passivating effects of the glyme ligands resulting in small nanoparticles and the imperfect packing of these nanocrystallites. It should be noted that the $NaYF_4$ materials prepared from the hydrothermal method exhibit a surface area of only 13.4 m^2 g^{-1}.[30] In contrast, the hexagonal phase shows a poor BET specific surface area (9.3 m^2 g^{-1}). Currently these $NaYF_4$ NCs are being tested as novel mixed-metal fluoride supports for the deposition of colloidal gold nanoparticles for the aerobic epoxidation of *t*-stilbene. Previous studies from this laboratory have shown that the single source precursor approach to get mixed-metal oxide supports for gold NPs results in better oxidation catalysts than the reference Au/TiO_2 catalyst from the World Gold Council.[31]

(e) Surface modification of as-prepared $NaYF_4$: 20% Yb^{3+}, 2% Er^{3+}/Tm^{3+} nanocrystals with hydrophilic ligands

Due to the presence of hydrophobic glyme ligands on the surface, the as-synthesized $NaYF_4$:Yb^{3+}, Er^{3+}/Tm^{3+} NCs are well dispersed in common organic solvents (C_7H_8, DMSO, CH_2Cl_2), the formed colloidal solutions being quite stable with no apparent agglomeration or settling for a period of several days under ambient conditions (Fig. 6). However, for bio-applications of these NCs, water solubility is crucial and thus, surface modifications of the as-prepared NCs have been performed during the course of this work to convert hydrophobic NCs into hydrophilic ones as well as to have some functional groups on their surfaces.[4] Previously, a method based on epoxidation of the surface oleic acid ligand, followed by coupling with polyethylene glycol monomethyl ether, has been described for converting hydrophobic up-converting nanoparticles into amphiphilic ones.[32] The strategy used here is a simple ligand-exchange reaction with polyacrylic acid (PAA) or polyethylene glycol (PEG) diacid 600, both of which serve as multidentate ligands that displace the original hydrophobic glymes on the surface of $NaYF_4$: Yb^{3+}, Er^{3+}/Tm^{3+} NCs and eventually render the NCs highly water soluble.[33] Fourier transform infrared (FT-IR) spectroscopy was used to characterize the functional groups present on the surface of the $NaYF_4$: Yb^{3+}, Er^{3+}/Tm^{3+} NCs before and after the ligand exchange. After ligand exchange by PEG diacid 600, the IR spectrum of NCs shows two strong bands at 1620 and 1454 cm^{-1}, which can be assigned to the asymmetric and symmetric stretching vibrations of carboxylic groups, respectively (Fig. 7). On the other hand, the IR spectrum of NCs capped by PAA shows two strong bands at 1722 and 1620 cm^{-1} for asymmetric stretching. Although this ligand-exchange process has no apparent effects on the shapes, sizes, and luminescent properties of the NCs, the PAA/PEG diacid

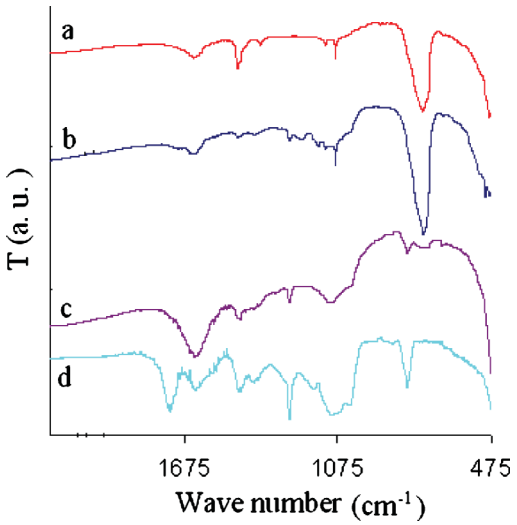

Fig. 7 FT-IR spectra of $NaYF_4$: Yb^{3+}, Er^{3+} NCs obtained at 250 °C and capped by diglyme (a), tetraglyme (b), PEG-diacid-600 (c), and PAA (d).

600-capped $NaYF_4$:Yb, Er^{3+}/Tm^{3+} NCs show good dispersibility in water, thus further suggesting that hydrophobic glymes have been replaced by hydrophilic PAA or PEG diacid 600 ligands. The presence of free carboxylic acid groups on their surfaces not only results in high solubility in water, but also allows further conjugation with various biomolecules, thus paving the way for potential bio-applications of the above up-converting NCs.[4]

(f) Elaboration and characterization of the $NaYF_4$: 20% Yb^{3+}, 2% $Er^{3+}(Tm^{3+})$ thin films

Since some of the promising applications of up-converting materials require thin films,[34] we evaluated the diglyme derivatives having correct stoichiometry of the two metals to elaborate $NaYF_4$:Yb^{3+}, Er^{3+} thin films by spin coating. A THF solution containing appropriate amounts of **1**, **4** and **6** (0.1 ml, 0.3–0.7 M L^{-1} concentration) were dropped rapidly on the pre-cleaned glass or Si substrate, spinning at a speed of 1200–2000 rpm for 30 s. The films were dried at 100 °C for 30 min and the whole procedure was repeated a few times to give the desired number of coatings. The films were finally annealed at 400 °C (10 °C min^{-1}) either in air or nitrogen atmosphere. These films were further analyzed by XRD, SEM and EDX measurements. The choice of substrate did not have any apparent effect on the nature of the crystallinity of the thin films. However, it was imperative to anneal the deposited films under an inert atmosphere to get the desired $NaY(Ln)F_4$ phase. The XRD patterns of the thin films deposited from **1**, **4** and **6** (2 coatings) on Si wafer and annealed under N_2 atmosphere at 400 °C for 4 h showed a hexagonal phase of $NaYF_4$ (Fig. 8). The chemical microanalysis performed using energy dispersive X-ray spectroscopy (EDX) further confirmed the composition of the annealed films being $NaYF_4$: 20%Yb^{3+}, ~2%Er^{3+} (Fig. S4a†). The film morphology was studied using scanning electron microscopy (SEM) studies, which showed it to be consisted of dense, spherical grains of average 1–2 μm size (Fig. 8a). In contrast, the X-ray diffraction pattern for the films deposited on glass and annealed at 400 °C for 4 h in air indicated the presence of mixed cubic phases YOF (JCPDS 04-008-3257) and NaF (JCPDS 01-070-2508) (Fig. 8d). This was further confirmed by EDX analysis

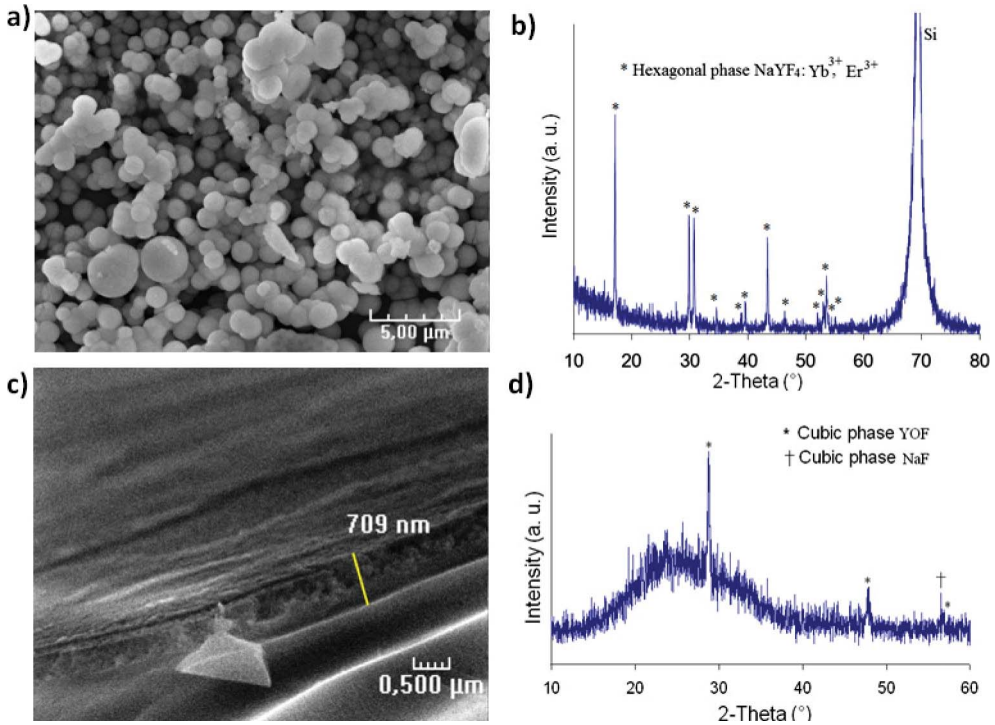

Fig. 8 Characterization of the thin films obtained by spin-coating of the diglyme precursors **1**, **4** and **6**. Above: SEM (a) and XRD (b) of the $NaYF_4$: Yb^{3+}, Er^{3+} films on Si wafer (calcined at 400 °C under nitrogen). Below: SEM (c) and XRD (d) of the NaF and Y(Ln)OF films on glass substrate (calcined at 400 °C in air).

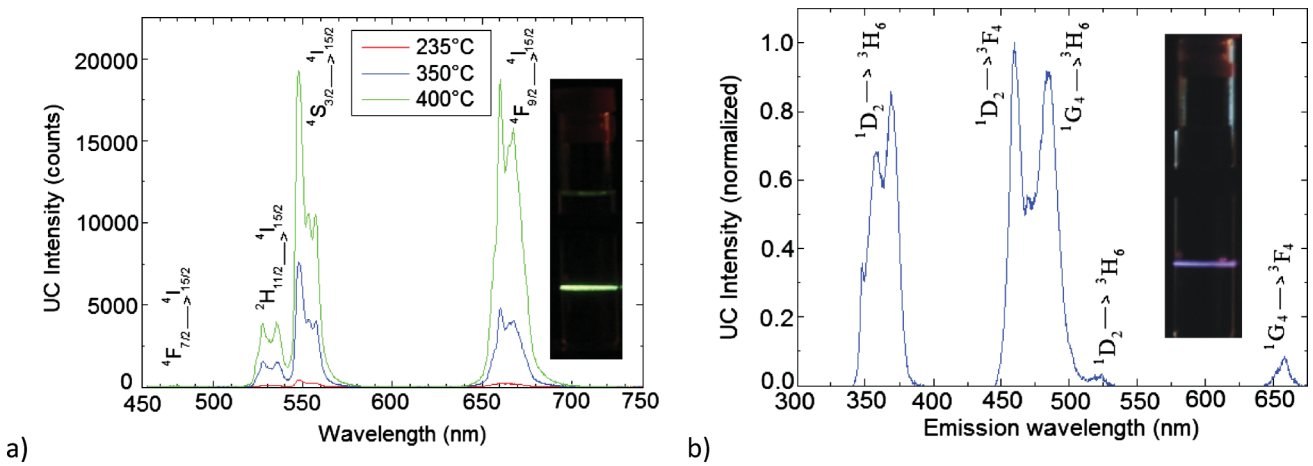

Fig. 9 a) Difference in up-conversion emission intensity of cubic and/or hexagonal phases of $NaYF_4$: 20% Yb^{3+}, 2% Er^{3+} NCs when taken as dry powder and excited at 970 nm (three samples as specified in Fig. 5b), and b) emission spectrum of $NaYF_4$: 20% Yb^{3+}, 2% Tm^{3+} NCs under similar conditions. The insets show digital photographs of the total up-conversion luminescence of above NCs taken as 1 wt % solutions in CH_2Cl_2.

(Fig. S4b†). The SEM images showed that these films, which were approximately 0.5 µm thick after 3 coatings, consisted of two apparent phases, a relatively smooth film along with some large crystallites (Fig. 8c). Deposition of somewhat porous and discontinuous up-converting thin films[35] using $NaY(Ln)F_4$ nanoparticles were recently reported. We show here that a more dense film can be produced using a precursor solution. A more detailed study involving different solvents, complexing reagents and concentrations of the precursor's solutions is currently under way to improve further the quality of above obtained films.

(g) Up-conversion studies

The up-conversion emission spectra of $NaYF_4$: 20% Yb^{3+}, 2% Er^{3+} and $NaYF_4$: 20% Yb^{3+}, 2% Tm^{3+} nanocrystals obtained at different temperatures and capped with different ligands were recorded in solid or solution states under 970 nm Ti-Sapphire laser excitation (8 W cm^{-2} power density) (Fig. 9). The emission bands in these spectra can easily be assigned to transitions within the 4f–4f levels of the Er^{3+} or Tm^{3+} ions in $NaYF_4$ host. Whereas the spectrum of the $NaYF_4$: 20% Yb^{3+}, 2% Er^{3+} sample exhibits classical green and red emission bands of Er^{3+} ion at 530–570 nm

($^2H_{11/2}$, $^4S_{3/2}$ → $^4I_{15/2}$ transitions) and 665 nm ($^4F_{9/2}$ → $^4I_{15/2}$ transition) (Fig. 9a), respectively, the sample co-doped with Yb^{3+} and Tm^{3+} ions shows classical blue and violet bands of Tm^{3+} ion at about 480 nm ($^1G_4$ → $^3H_6$), 460 nm ($^1D_2$ → $^3F_4$) and 370 nm ($^1D_2$ → $^3H_6$) as well as a weak red emission at about 665 nm ($^3F_3$ → $^3H_6$) (Fig. 9b). The $NaYF_4$ nanomaterials co-doped with Yb^{3+}/Er^{3+}ions show a yellowish green total luminescence due to a combination of green and red emissions, whereas a blue total luminescence is observed for the samples containing Yb^{3+}/Tm^{3+} ions as dopants (the digital images of the total up-conversion luminescence of the NCs taken as 1 wt% colloidal solutions in dicholoromethane are shown as insets in Fig. 9a & 9b). It is clear from these figures that i) the up-conversion efficiency is better for the hexagonal phase than the cubic phase (Fig. 9a), ii) the shape of emission spectra remains same irrespective of whether the NCs are taken in solid or solution states (Fig. S5†), though the global measured intensity is lower in solution due to grain dispersion, functionalization, *etc.*, and iii) the NCs are stable for months when kept in the dichloromethane but are slowly destroyed in the water (Fig. 10, S6†). That the sensitization of Er^{3+} ion by Yb^{3+} ion (by transferring its absorption $^2F_{7/2}$→$^2F_{5/2}$ to the former) occurs during the above UC process is clearly indicated by the excitation spectra shown in Fig. 11a where a broad absorption is observed for $NaYF_4$ NCs co-doped with Yb^{3+} and Er^{3+} ions as against the Er^{3+} $^2F_{7/2}$ → $^2F_{5/2}$ narrow absorption when particles were doped with the Er^{3+} ion only. The Fig. 11b shows that the order of magnitude of this sensitization is more than three.

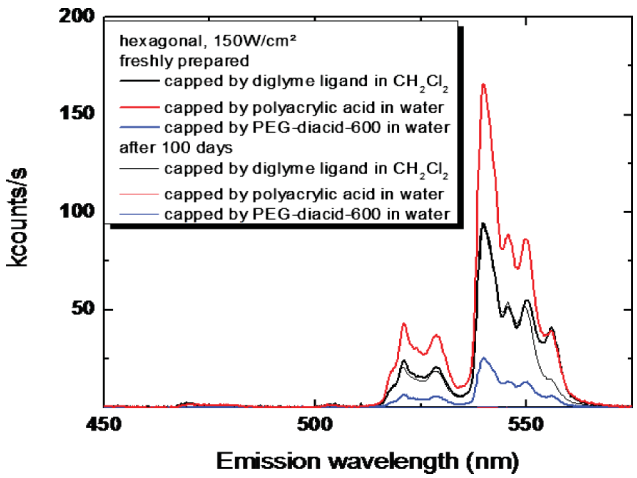

Fig. 10 Effect of aging of $NaYF_4$: 20% Yb^{3+}, 2% Er^{3+} NCs. The emission spectra for the hydrophilic NCs in water after 100 days are poorly visible in the figure due to very low intensity.

In order to determine the numbers of photons responsible for the up-conversion mechanism, the intensities of the up-conversion emissions were recorded as a function of the 970 nm excitation intensity (Fig. 12, S7†). At low power, the power dependencies of the green and red up-conversion emission intensities of Er^{3+} (from $^4S_{3/2}$ & $^2H_{11/2}$) and blue emission intensity of Tm^{3+} (from $^1G_4$) were found to be approximately two, indicating that 2 IR excitation photons were involved in the up-conversion mechanism. On the other hand, the violet emissions (from $^2H_{9/2}$ & $^4G_{11/2}$ for Er^{3+} and $^1D_2$ for Tm^{3+}) involved a process that required 3 IR photons (Fig. 12). At high excitation densities (above 40 mW cm^{-2}), the saturation of the energy transfer processes occurs. The UC, which is a nonlinear process, does not maintain its nonlinear behavior up to infinite excitation energies. At high excitation densities, due to sample heating, a relative enhancement of the intensity from $^2H_{11/2}$ & $^4G_{11/2}$ levels was also observed.

The so-called green to red ratio (GRR) is usually considered as an indicator to define the efficiency of the up-converting samples.[36] Fig. 13 shows the evolution of the GRR as a function of the incident fluence on both cubic and hexagonal phases of $NaYF_4$:Yb^{3+}, Er^{3+} NCs. Here we have plotted exclusively the relative intensity ratios of $^4S_{3/2}$ → $^4I_{15/2}$ and $^4F_{9/2}$ → $^4I_{15/2}$ emissions. As power increases, the GRR first increases also and then becomes constant for the cubic phase of the above UC materials. In contrast, a slight decrease in the GRR is observed for the hexagonal phase. This opposite behavior for the two phases underlines the necessity to be more careful while using GRR as a general indicator to define up-converting efficiency. Besides the crystallographic phase and excitation power, the GRR values can also be influenced by several other factors such as doping levels of rare earth ions, energy gap resonances, preparative routes, crystallinity, capping ligands and surface defects.

The up-conversion excitation pathways for the Er^{3+}/Yb^{3+} co-doped materials are well known and are shown in Fig. 14. In this case, an initial energy transfer up-conversion (ETU) from an Yb^{3+} ion in the $^2F_{5/2}$ state to an Er^{3+} ion populates the $^4I_{11/2}$ level. A second energy transfer from an Yb^{3+} ion can then populate the $^4F_{7/2}$ level of the Er^{3+} ion. The Er^{3+} ion can then relax by a non-radiative transition to the $^2H_{11/2}$ and $^4S_{3/2}$ levels, and the green $^2H_{11/2}$ → $^4I_{15/2}$ and $^4S_{3/2}$ → $^4I_{15/2}$ emissions occur. Different ways can be involved to populate $^4F_{9/2}$, the state at the origin of the red emission: non-radiative relaxation from $^4S_{3/2}$, cross relaxation between two Er^{3+} ions in $^4S_{3/2}$ state or $^4I_{11/2}$ state, respectively, or ETU from an Yb^{3+} ion in $^2F_{5/2}$ state to an Er^{3+} ion in $^4I_{13/2}$ level. On the other hand, the UC excitation pathways for $NaYF_4$: Tm^{3+}, Yb^{3+} NCs seem to be slightly different in our case than those reported in the literature.[9] For instance Heer *et al.* reported a dependency (with fluence) of the fourth order for $^1D_2$ → $^3H_6$ emission and of the third order for the $^1G_4$ → $^3H_6$ emission.[9] However, in our experiments we found above emissions of third and second order, respectively. To understand our results, we have to invoke a process of cooperative sensitization and energy transfer up-conversion as shown in Fig. 14b. In this case, two excited Yb^{3+} ions transfer simultaneously their excitation to one Tm^{3+} ion. This process seems reasonable in this case since there is a very good matching of the energy of the $^1G_4$ level of Tm^{3+} ion with twice the Yb^{3+} $^4F_{5/2}$ energy. ETU involving the Yb^{3+} ion excited in $^4F_{5/2}$ and the Tm^{3+} ion excited in $^1G_4$ could then lead to the population of $^1D_2$ level. A more detailed study involving samples with various amounts of Yb^{3+} ions is currently under way to validate this interpretation.

Experimental

All reactions were carried out under argon using Schlenk tube and vacuum line techniques. $Ln(TFA)_3(H_2O)_3$ were prepared by reacting the Ln_2O_3 with trifluoroacetic acid in refluxing toluene. Trifluoroacetic acid (TFAH) and glymes (all Aldrich) were stored over molecular sieves. Solvents were purified on an MB SPS-800 instrument. FT-IR spectra were recorded as Nujol mulls on a Bruker Vector 22 spectrometer. ^1H NMR spectra were

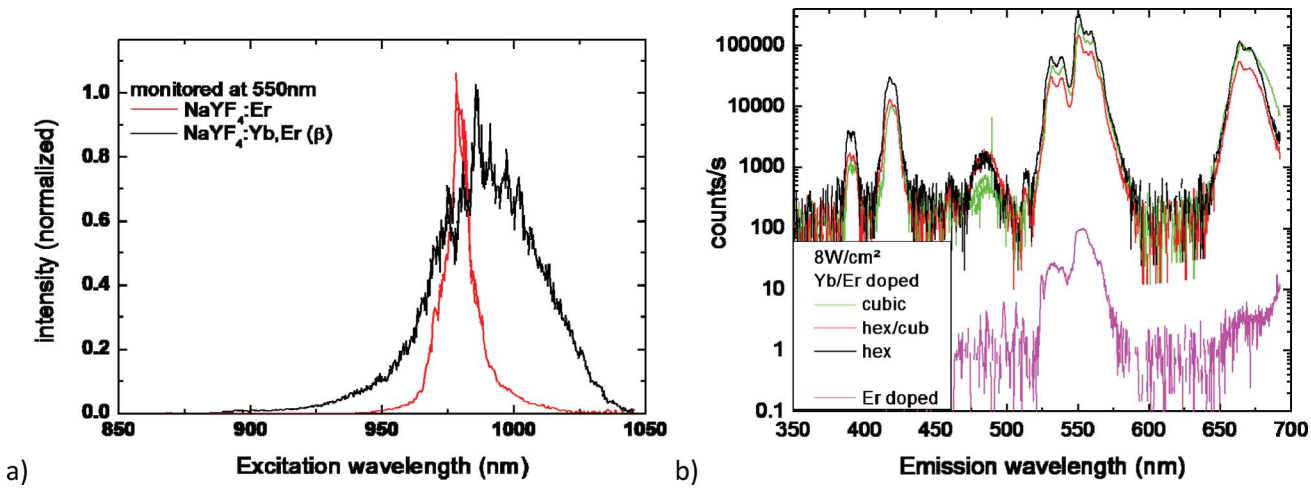

Fig. 11 Excitation (a) and emission spectra (b) of the $NaYF_4$: Er^{3+} and $NaYF_4$: Yb^{3+}, Er^{3+} NCs showing sensitization of Er^{3+} by Yb^{3+}.

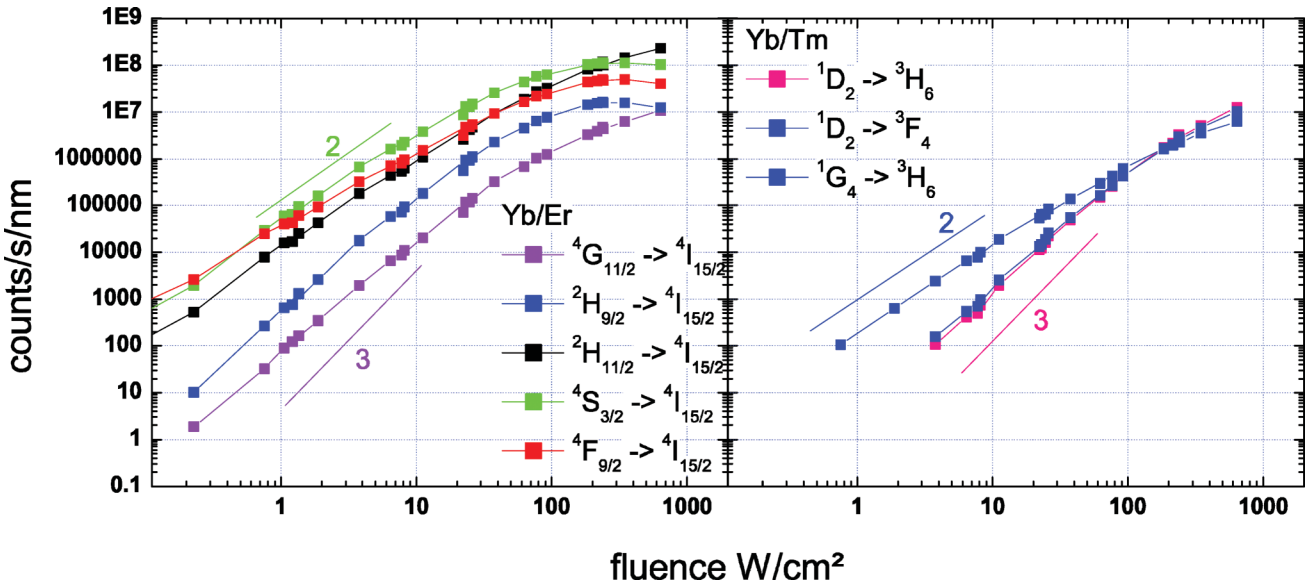

Fig. 12 Evolution of the intensity of the difference bands of the cubic phase of $NaYF_4$: Yb^{3+}, Ln^{3+} NCs with the excitation power: Ln = Er (a), Tm (b).

registered on a Bruker AC-300 spectrometer. TG-DTA data for the derivatives **1–3** and $Y(TFA)_3(H_2O)_3$ were collected in argon atmosphere (flow rate 50 cm^3 min^{-1}, thermal ramp 5 °C min^{-1}, temperature range 20–600 °C) using a SETSYS Evolution-12 thermal analyzer, whereas those of as-prepared $NaYF_4$:Yb^{3+}, Er^{3+}/Tm^{3+} NCs were recorded on a Setaram 92 system in air with a thermal ramp of 5 °C min^{-1}. Analytical data were obtained from the Service Central d'Analyses du CNRS. SEM images of thin films were collected on Hitachi S800 spectrometers. The glass substrates and Si wafers were cleaned with acetone and dried at 120 °C prior to use. Up-conversion measurements were performed by using a coherent 899 ring Ti-Sapphire laser pumped by an Argon laser (514 nm) from coherent (innova 300), delivering a power of 8 W. The Ti-Sapphire line can be tuned from 880 to 1060 nm. The average maximum power sent to the sample over this wavelength ranges from 25 to 200 mW. The laser is focused on the sample on a 150 μm diameter spot. The up-conversion luminescence was collected by an optical fiber and connected to a Jobin-Yvon TRIAX 320 monochromator and equipped with a CCD2000 charge coupled device. The light is dispersed with a 300 groove mm^{-1} grating ensuring a resolution better than 2 nm. For the excitation spectra the light was also collected with the CCD and afterward integrated over the wavelength range of interest. The same is true for the variation as a function of power. For this last case the power was varied by interposing neutral filters on the beam. A quartz plate was interposed on the beam after the density filter, and the reflection was sent to a power meter (1931-C from Newport) in order to monitor the power at all instants. Emission and excitation spectra were performed at 1.5 mW (approximately 8 W cm^{-2}) in the linear range.

Synthesis of 1–8

Due to the similarity in preparative method, only the synthesis of complex **3** is described in detail. The other complexes **1**, **2** and **4–8** were prepared using similar procedure and crystallized from a 1 : 4 mixture of THF and Et_2O. For these complexes, therefore, only the reactants and their quantity (in brackets) are shown below:

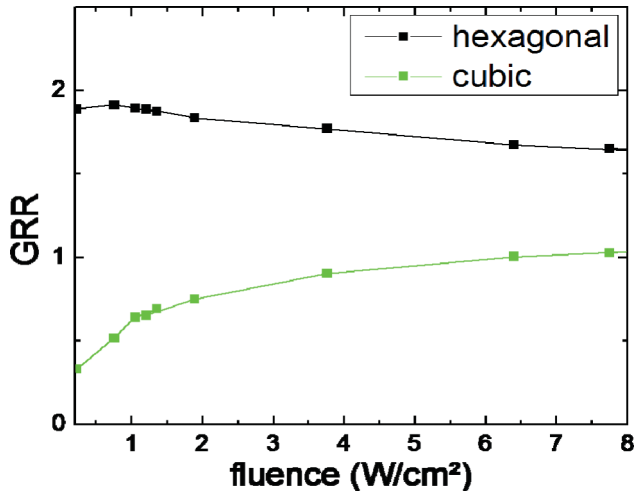

Fig. 13 Excitation density dependence of the green to red ratio.

[$YNa_2(TFA)_5$(tetraglyme)] (3·0.5Et_2O). A freshly prepared THF solution (7 ml) of NaTFA [NaH (0.04 g, 1.64 mmol) and TFAH (0.13 ml, 1.65 mmol)] was added drop wise to a solution of $Y(TFA)_3(H_2O)_3$ (0.79 g, 1.63 mmol) in 10 ml of THF. After 10 min, tetraglyme (0.72 ml, 3.26 mmol) was added and the resulting solution was stirred for 4 h at room temperature. Removal of solvents afforded a colorless vicious residue, which was washed twice with n-hexane. The residue was dissolved in 2 ml of THF and layered carefully with 10 ml of diethyl ether. Colorless blocks grew overnight (0.75 g, 94% based on NaH). The reaction in the right stoichiometry [NaH (0.09 g, 3.91 mmol) and TFAH (0.13 ml, 1.66 mmol) $Y(TFA)_3(H_2O)_3$ (0.8 g, 1.66 mmol), tetraglyme (0.38 ml, 1.72 mmol)] improved the yield of the product (1.53 g, 96%). Depending on time period of drying of **3** under *vacuo*, half-to-complete solvated diethyl ether molecules were lost. Anal. Calcd. for $C_{20}H_{22}F_{15}Na_2O_{15}Y·0.5C_4H_{10}O$ (959): C, 27.52; H, 2.81; Na, 4.79; Y, 9.28. Found: C, 26.77.; H, 2.62; Na, 4.85; Y, 9.45%. FT-IR (Nujol, cm^{-1}): 1735 s, 1684 s ($\nu_{as}CO_2$), 1458 s, 1360 s, 1349 s, 1209 s, 1140 s (ν_{C-F}, ν_{C-O}), 1082 s, 1042 m, 944 m, 848 s, 797 s, 722 s, 607 m, 522 m, 456 m, 440m. ^{1}H NMR (CD_3CN, ppm): 1.0 (t, J = 6.8 Hz, 1.5H, CH_3 of ether), 3.3 (q, J = 6.8 Hz, 1H, CH_2 of ether), 3.60 (s, 6H, OMe), 3.80, 3.90 (s, 16H, OCH_2).

[NaY(TFA)$_4$(diglyme)] (1). NaH (0.033 g, 1.37 mmol), TFAH (0.10 ml, 1.32 mmol) and $Y(TFA)_3(H_2O)_3$ (0.64 g, 1.33 mmol). Yield, 0.86 g (94%). Anal. Calcd. for $C_{14}H_{14}F_{12}NaO_{11}Y$ (698.1): C, 24.01; H, 2.0; Na, 3.29; Y, 12.75. Found: C, 24.01; H, 2.10; Na, 3.26; Y, 12.75%. FT-IR (Nujol, cm^{-1}): 1784 m, 1683 m ($\nu_{as}CO_2$), 1462 s, 1376 s, 1223 m, 1204 m, 1148 m (ν_{C-F}, ν_{C-O}), 1092w, 1019w, 940w, 870w, 846 m, 796 m, 723 s, 607 m, 523 m, 455 m, 439m. ^{1}H NMR (CD_3CN, ppm): 3.5 (s, 6H, OMe), 3.7, 3.8 (s, 8H, OCH_2).

[Na(triglyme)$_2$][$Y_2(TFA)_7(THF)_2$] (2). NaH (0.035 g, 1.46 mmol), TFAH (0.11 ml, 1.40 mmol) and $Y(TFA)_3(H_2O)_3$ (0.67 g, 1.39 mmol). Yield, 1.87 g, 87%. A better yield of the product (0.83 g, 93%) was obtained using the right stoichiometry of the reactants [NaH (0.015 g, 0.62 mmol) and TFAH (0.05 ml, 0.65 mmol) $Y(TFA)_3(H_2O)_3$ (0.58 g, 1.20 mmol), triglyme (0.22 ml, 1.21 mmol)]. Anal. Calcd. for $C_{38}H_{52}F_{21}Na_1O_{24}Y_2$ (1492.6): C, 30.55; H, 3.48; Na, 1.54; Y, 11.92. Found: C, 30.40; H, 3.45; Na, 1.55; Y, 12.0%. FT-IR (Nujol, cm^{-1}): 1759 s, 1681 s ($\nu_{as}CO_2$), 1462 s, 1376 m, 1331 m, 1211 s, 1146 s (ν_{C-F}, ν_{C-O}), 1099 s, 1048 m, 1027 m, 946w, 933w, 920w, 871w, 847 m, 796 m, 723 s, 609 m, 523 m, 452 m, 440 m, 408w. ^{1}H NMR (CD_3CN, ppm): 1.9

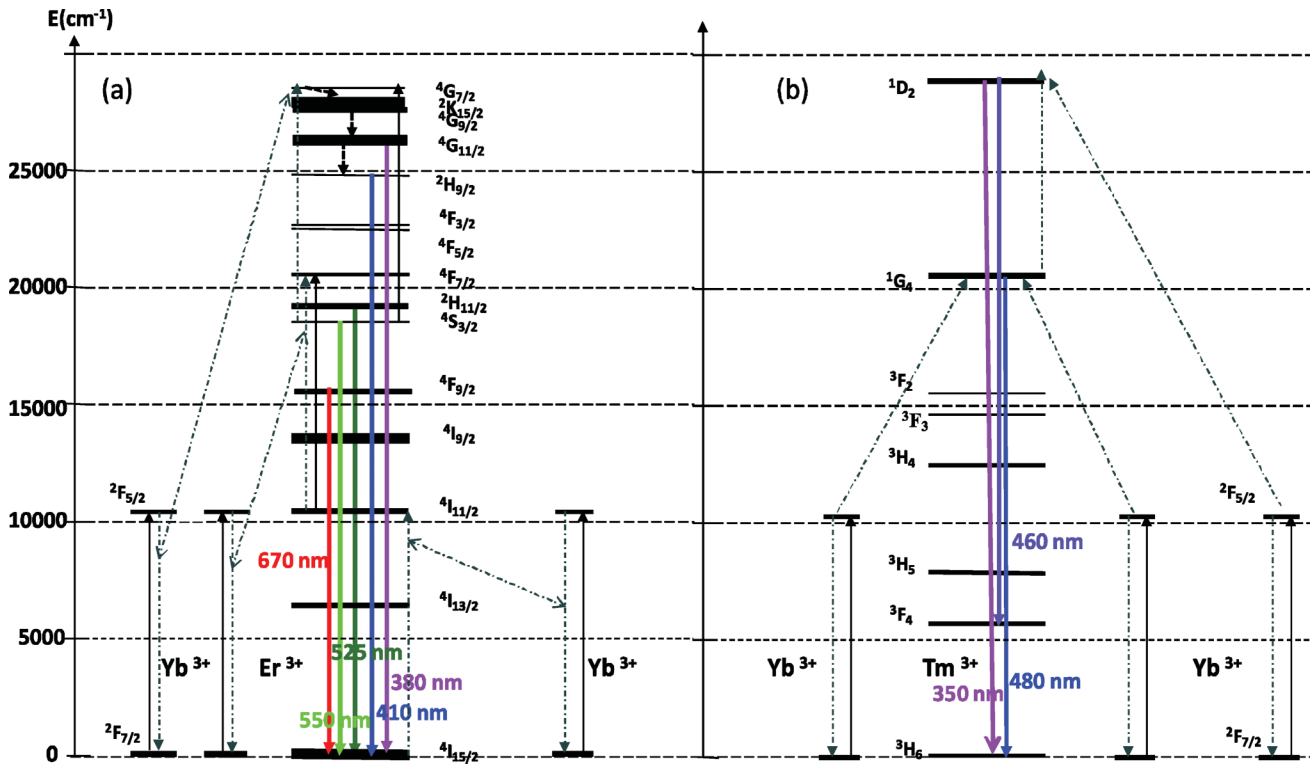

Fig. 14 Schematic energy level diagrams showing cooperative sensitization and energy transfer up-conversion for the Yb^{3+}, Er^{3+} and Yb^{3+}, Tm^{3+} systems.

(m, J = 6.8 Hz, 8H, α-CH_2 of THF), 2.9 (s, 12 H, OMe), 3.4, 3.5 (s, 24 H, OCH_2), 3.7 (m, J = 6.8 Hz, 8H, β-CH_2 of THF).

[NaEr(TFA)$_4$(diglyme)] (4). NaH (0.039 g, 1.62 mmol), TFAH (0.12 ml, 1.60 mmol), Er(TFA)$_3$(H_2O)$_3$ (0.86 g, 1.53 mmol), diglyme (0.22 ml, 1.55 mmol). Yield, 1.06 g (89%). Anal. Calcd. for $C_{14}H_{14}F_{12}ErNaO_{11}$ (776.3): C, 21.64; H, 1.80; Na, 2.96; Er, 21.55. Found: C, 21.61; H, 1.80; Na, 2.98; Er, 21.62%. FT-IR (Nujol, cm^{-1}): 1746 s, 1682 s ($\nu_{as}CO_2$), 1456 s, 1422 s, 1378 s, 1355 s, 1243 s, 1154 s (ν_{C-F}, ν_{C-O}), 1017 m, 862 s, 836 s, 800 s, 722 s, 605 m, 521 s, 454 m, 436 m.

[NaTm(TFA)$_4$(diglyme)] (5). NaH (0.108 g, 4.50 mmol), TFAH (0.35 ml, 4.60 mmol), Tm(TFA)$_3$(H_2O)$_3$ (2.525 g, 4.50 mmol), diglyme (0.65 ml, 4.54 mmol). Yield, 3.26 g (93%). Anal. Calcd. for $C_{14}H_{14}F_{12}NaO_{11}Tm$ (777.9): C, 21.56; H, 1.79; Na, 2.95; Tm, 21.68. Found: C, 21.62; H, 1.81; Na, 2.92; Tm, 21.60%. FT-IR (Nujol, cm^{-1}): 1786 s, 1679 s ($\nu_{as}CO_2$), 1461 s, 1422w, 1377 m, 1354 m, 1217 s, 1149 s (ν_{C-F}, ν_{C-O}), 1086 s, 1018 m, 990 w, 944 w, 871 m, 845 m, 797 s, 722 s, 607 m, 522 m, 455 m, 438 m.

[NaYb(TFA)$_4$(diglyme)] (6). NaH (0.03 g, 1.33 mmol), TFAH (0.10 ml, 1.31 mmol), Yb(TFA)$_3$(H_2O)$_3$ (0.73 g, 1.29 mmol), diglyme (0.20 ml, 1.39 mmol). Yield, 0.98 g (97%). Anal. Calcd. for $C_{14}H_{14}F_{12}NaO_{11}Yb$ (782): C, 21.35; H, 1.78; Na, 2.92; Yb, 21.98. Found: C, 21.39; H, 1.81; Na, 2.90; Yb, 22.04%.FT-IR (Nujol, cm^{-1}): 1735 s, 1682 s ($\nu_{as}CO_2$), 1457 s, 1432w, 1372 m, 1355 m, 1212 s, 1149 s (ν_{C-F}, ν_{C-O}), 1085 s, 1017 m, 946w, 863 m, 837 m, 800 m, 722 s, 606 m, 521 m, 456 m, 422 w.

[Na$_2$Er(TFA)$_5$(tetraglyme)] (7·0.5Et$_2$O). NaH (0.039 g, 1.62 mmol) and TFAH (0.13 ml, 1.68 mmol), Er(TFA)$_3$(H_2O)$_3$ (0.45 g, 0.80 mmol), tetraglyme (0.18 ml, 0.82 mmol). Yield, 0.76 g (91%). Anal. Calcd. for $C_{20}H_{22}F_{15}Na_2O_{15}Er{\cdot}0.5C_4H_{10}O$ (1036.7): C, 23.15; H, 2.12; Na, 4.43; Er, 16.13. Found: C, 23.27; H, 2.16; Na, 4.39; Er, 16.0%. FT-IR (Nujol, cm^{-1}): 1730 s, 1680 s ($\nu_{as}CO_2$), 1455 s, 1358 s, 1345 s, 1207 s, 1138 s (ν_{C-F}, ν_{C-O}), 1080 s, 1040 m, 940 m, 845 s, 794 s, 720 s, 605 m, 520 m, 455 m, 435 m.

[Na$_2$Yb(TFA)$_5$(tetraglyme)] (8·0.5Et$_2$O). NaH (0.20 g, 0.82 mmol) and TFAH (0.06 ml, 0.82 mmol), Yb(TFA)$_3$(H_2O)$_3$ (0.23 g, 0.40 mmol), tetraglyme (0.1 ml, 0.45 mmol). Yield, 0.4 g (95%). Anal. Calcd. for $C_{20}H_{22}F_{15}Na_2O_{15}Yb{\cdot}0.5C_4H_{10}O$ (1040.8): C, 23.06; H, 2.11; Na, 4.41; Yb, 16.62. Found: C, 23.0.; H, 2.07; Na, 4.35; Yb, 16.54%. FT-IR (Nujol, cm^{-1}): 1733 s, 1682 s ($\nu_{as}CO_2$), 1458 s, 1359 s, 1347 s, 1210 s, 1136 s (ν_{C-F}, ν_{C-O}), 1082 s, 1042 m, 944 m, 846 s, 798 s, 721 s, 608 m, 521 m, 456 m, 442 m.

X-ray crystallography of 2 and 3

Suitable crystals of **2** and **3** were mounted on an Oxford-Diffraction Gemini diffractometer equipped with an Atlas CCD detector and a Nonius Kappa CCD diffractometer, respectively. For **2**, the intensities were collected at 180 K by means of the CrysalisPro software,[37] whereas data for **3** were recorded using MoK_λ radiation (λ = 0.71073 Å) at 150 K by means of the COLLECT software.[38] Reflection indexing, Lorentz-polarization correction, peak integration and background determination were carried out with CrysalisPro[37] (for **2**) and DENZO[39] (for **3**). Frame scaling and unit-cell parameters refinement were made with SCALEPACK.[39] A multi-scan (for **2**)[40] or analytical (for **3**)[41] absorption correction was applied. The structures were solved by direct methods with SIR97,[42] whereas the structural refinement was carried out with CRYSTALS.[43] Some of the fluorine atoms in **2** and **3** showed high thermal motion due to rotational disorder of the CF_3 moiety.

Preparation and characterization of $NaYF_4$: 20% Yb^{3+}, 2% Er^{3+}/Tm^{3+} nanocrystals

The diglyme and tetraglyme precursors start decomposing at 250 and 235 °C, respectively, to give $NaYF_4$ nanocrystals. A typical method of obtaining $NaYF_4$: 20% Yb^{3+}, 2% Er^{3+}/Tm^{3+} nanocrystals involves taking suitable complexes (**1** + **4** + **6**, **1** + **5** + **6** or **3** + **7** + **8**) in corresponding amounts in high-boiling solvent 1-octadecene (15 ml) and heating gradually at a rate of 10 °C min^{-1} under argon. After refluxing at the selected temperature (235–315 °C) for 1 h, the mixture was allowed to cool to room temperature and nanoparticles were then precipitated by adding ethanol and isolated *via* centrifugation. The obtained NCs were then washed twice by dispersing in ethanol, centrifuged and dried in an oven at 70 °C (24 h).

Surface modification

The as-synthesized glyme-capped hydrophobic $NaYF_4$:Yb^{3+}, Er^{3+} NCs were modified to have hydrophilic surfaces by replacing glyme ligand with either poly acrylic acid (PAA) or polyethylene glycol 600 diacid ligand by using the procedures described in the literature.[33] After ligand exchange, the nanoparticles formed a clear colloidal solution in deionized water. These solutions remained clear for several days and no noticeable settling or precipitation was observed.

Conclusions

We reported here well-characterized Na-Y(Ln) heterobi-metallic derivatives with trifluoroacetate and glyme ligands as first single source precursors for up-converting $NaYF_4$:Yb^{3+}, Er^{3+}/Tm^{3+} nanocrystals and thin films. Compared to the extensively used homometallic trifluoroacetate precursors, the above heterometallics offer many inherent advantages such as those mentioned in the Introduction section. The $NaYF_4$:20% Yb^{3+}, 2% Er^{3+} and $NaYF_4$:20% Yb^{3+}, 2% Tm^{3+} nanocrystals produced using these precursors were sub-25 nm in diameter with a narrow size distribution, which efficiently up-converted NIR light into red/green and blue/violet light. We believe that the easy-to-scale up synthetic pathway reported here, not requiring sophisticated equipment or complicated procedures and using technical grade solvents/ligands and yet producing highly luminescent and uniform NCs, could be extended as a general strategy to prepare other heterometal fluorides such as $MLnF_4$ (M = Li, K), $NaMF_3$ (M = late transition metals) and $LiMAlF_6$ (M = Ca, Sr)[44] as high-tech materials.

Acknowledgements

We gratefully acknowledge the help extended by B. Jouguet (TG-DTA of **1–3**), M. Daniel (TEM and SEM) and F. Bosselet (XRD) of IRCELYON during the course of this work.

References

1 F. Auzel, *Chem. Rev.*, 2004, **104**, 139.
2 J. F. Suyver, A. Aebischer, D. Biner, P. Gerner, J. Grimm, S. heer, K. W. Kramer, C. Reinhard and H. U. Gudel, *Opt. Mater.*, 2005, **27**, 1111.
3 F. Wang and X. Liu, *Chem. Soc. Rev.*, 2009, **38**, 976.
4 F. Wang, D. Banerjee, Y. Liu, X. Chen and X. Liu, *Analyst*, 2010, **135**, 1839; J.-C. Boyer, M.-P. Manseau, J. I. Murray and F. C. J. M. Van Veggel, *Langmuir*, 2010, **26**, 1157; D. K. Chatterjee, A. J. Rufaihah and Y. Zhang, *Biomaterials*, 2008, **29**, 937; R. A. Jalil and Y. Zhang, *Biomaterials*, 2008, **29**, 4122.
5 J. Zhou, Y. Sun, X. Du, L. Xiong, H. Hu and F. Li, *Biomaterials*, 2010, **31**, 3287; M. Yu, F. Li, Z. Chen, H. Hu, C. Zhan, H. Yang and C. Huang, *Anal. Chem.*, 2009, **81**, 930; L. Xiong, Z. Chen, Q. Tian, T. Cao, C. Xu and F. Li, *Anal. Chem.*, 2009, **81**, 8687; S. F. Lim, R. Riehn, W. S. Ryu, N. Khanarian, C. K. Tung, D. Tank and R. H. Austin, *Nano Lett.*, 2006, **6**, 169; P. Zhang, S. Rogelj, K. Nguyen and D. Wheeler, *J. Am. Chem. Soc.*, 2006, **128**, 12410.
6 C. Li and J. Lin, *J. Mater. Chem.*, 2010, **20**, 6831; Z. Q. Li, Y. Zhang and S. Jiang, *Adv. Mater.*, 2008, **20**, 4765; Z. G. Chen, H. L. Chen, H. Hu, M. X. Yu, F. Y. Li, Q. Zhang, Z. G. Zhou, T. Yi and C. H. Huang, *J. Am. Chem. Soc.*, 2008, **130**, 3023; J. Shen, L.-D. Sun and C.-H. Yan, *Dalton Trans.*, 2008, 5687; R. H. Page, K. I. Schaffers, P. A. Waide, J. B. Tassano, S. A. Payne, W. F. Krupke and W. K. Bischel, *J. Opt. Soc. Am. B*, 1998, **15**, 996.
7 F. Wang, Y. Han, C. S. Lim, Y. Lu, J. Wang, J. Xu, H. Chen, C. Zhang, M. Hong and X. Liu, *Nature*, 2010, **463**, 1061.
8 N. Menyuk, K. Dwight and J. W. Pierce, *Appl. Phys. Lett.*, 1972, **21**, 159.
9 S. Heer, K. Kompe, H. Gudel and M. Haase, *Adv. Mater.*, 2004, **16**, 2102.
10 G. Yi, H. Lu, S. Zhao, Y. Ge, W. Yang, D. Chen and L.-H. Guo, *Nano Lett.*, 2004, **4**, 2191.
11 J. Jhuang, J. Wang, X. Yang, I. D. Williams, W. Zhang, Q. Zhang, Z. Feng, Z. Yang, C. Liang, M. Wu and Q. Su, *Chem. Mater.*, 2009, **21**, 160; C. Li, C. Zhang, Z. Hou, L. Wang, Z. Quan, H. Lian and J. Lin, *J. Phys. Chem. C*, 2009, **113**, 2332; L. Wang and Y. Li, *Chem. Commun.*, 2006, 2557; J. Zeng, J. Su, Z. Li, R. Yan and Y. Li, *Adv. Mater.*, 2005, **17**, 2119; L. Wang, R. Yan, Z. Huo, L. Wang, J. Zeng, J. Bao, X. Wang, Q. Peng and Y. Li, *Angew. Chem., Int. Ed.*, 2005, **44**, 6054.
12 C. Liu, H. Wang, X. Li and D. Chen, *J. Mater. Chem.*, 2009, **19**, 3546; Y. Wei, F. Q. Lu, X. R. Zhang and D. Chen, *Chem. Mater.*, 2006, **18**, 5733.
13 L. Wang and Y. Li, *Chem. Mater.*, 2007, **19**, 727; L. Wang and Y. Li, *Nano Lett.*, 2006, **6**, 1645.
14 X. Liu, J. Zhao, Y. Sun, K. Song, Y. Yu, C. Du, X. Kong and H. Zhang, *Chem. Commun.*, 2009, 6628.
15 H.-Q. Wang and T. Nann, *ACS Nano*, 2009, **3**, 3804.
16 S. Mishra, E. Jeanneau, M. H. Berger, J.-F. Hochepied and S. Daniele, *Inorg. Chem.*, 2010, **49**, 11184; S. Mishra, E. Jeanneau and S. Daniele, *Polyhedron*, 2010, **29**, 500; S. Mishra, S. Daniele, S. Petit, E. Jeanneau and M. Rolland, *Dalton Trans.*, 2009, 2569; S. Mishra, S. Daniele and L. G. Hubert-Pfalzgraf, *Chem. Soc. Rev.*, 2007, **36**, 1770; L. G. Hubert-Pfalzgraf, *Inorg. Chem. Commun.*, 2003, **6**, 102.
17 W. Niu, S. Wu, S. Zhang and L. Li, *Chem. Commun.*, 2010, **46**, 3908; C. Chen, L.-D. Sun, Z.-X. Li, L.-L. Li, J. Zhang, Y.-W. Zhang and C.-H. Yan, *Langmuir*, 2010, **26**, 8797; J. C. Boyer, L. A. Cuccia and J. A. Capobianco, *Nano Lett.*, 2007, **7**, 847; G. S. Yi and G. M. Chow, *Chem. Mater.*, 2007, **19**, 341; J. Shan, X. Qin, N. Yao and Y. Ju, *Nanotechnology*, 2007, **18**, 445607; J. Shan and Y. Ju, *Appl. Phys. Lett.*, 2007, **91**, 123103; H.-X. Mai, Y.-W. Zhang, R. Si, Z.-G. Yan, L.-D. Sun, L.-P. You and C.-H. Yan, *J. Am. Chem. Soc.*, 2006, **128**, 6426; J. C. Boyer, F. Vetrone, L. A. Cuccia and J. A. Capobianco, *J. Am. Chem. Soc.*, 2006, **128**, 7444.
18 S. Mishra, S. Daniele, G. Ledoux, E. Jeanneau and M. F. Joubert, *Chem. Commun.*, 2010, **46**, 3756.
19 A. Navulla, A. A. Tsirlin, A. M. Abakumov, R. V. Shpanchenko, H. Zhang and E. V. Dikarev, *J. Am. Chem. Soc.*, 2011, **133**, 692.
20 S. Mishra, L. G. Hubert-Pfalzgraf, S. Daniele, M. Rolland, E. Jeanneau and B. Jouguet, *Inorg. Chem. Commun.*, 2009, **12**, 97; J. Zhang, S. Morlens, L. G. Hubert-Pfalzgraf and D. Luneau, *Eur. J. Inorg. Chem.*, 2005, 3928.
21 G. B. Deacon and R. J. Phillips, *Coord. Chem. Rev.*, 1980, **33**, 227.
22 S. Mishra, J. Zhang, L. G. Hubert-Pfalzgraf, D. Luneau and E. Jeanneau, *Eur. J. Inorg. Chem.*, 2007, 602.
23 S. Mishra, E. Jeanneau, S. Daniele, G. Ledoux and P. N. Swamy, *Inorg. Chem.*, 2008, **47**, 9333; S. Mishra, E. Jeanneau, S. Daniele and L. G. Hubert-Pfalzgraf, *CrystEngComm*, 2008, **10**, 814.
24 C. W. Haigh, *Polyhedron*, 1996, **15**, 605.
25 K. Izod, S. T. Liddle and W. Clegg, *Inorg. Chem.*, 2004, **43**, 214.
26 S. Mishra, L. G. Hubert-Pfalzgraf and E. Jeanneau, *Polyhedron*, 2007, **26**, 66; H. Bock, C. Nather, Z. Havalas, A. John and C. Arad, *Angew. Chem., Int. Ed. Engl.*, 1994, **33**, 875.
27 W. A. Wojtczak, P. Atanassova, M. J. Hampden-Smith and E. Duesler, *Inorg. Chem.*, 1996, **35**, 6995.
28 J. A. Samuels, J. W. Zwanziger, E. B. Lobkovsky and K. G. Caulton, *Inorg. Chem.*, 1992, **31**, 4046; D. C. Bradley, M. Hasan, M. B. Hursthouse, M. Motevalli, O. F. Z. Khan, R. G. Pritchard and J. O. Williams, *J. Chem. Soc., Chem. Commun.*, 1992, 575; H. Vincent, F. Labrize and L. G. Hubert-Pfalzgraf, *Polyhedron*, 1994, **13**, 3323.
29 J. Shan and Y. Ju, *Nanotechnology*, 2009, **20**, 275603; H.-X. Mai, Y.-W. Zhang, L.-D. Sun and C.-H. Yan, *J. Phys. Chem. C*, 2007, **111**, 13730.
30 J. Zhao, X. Liu, D. Cui, Y. Sun, Y. Yu, Y. Yang, C. Du, Y. Wang, K. Song, K. Liu, S. Lu, X. Kong and H. Zhang, *Eur. J. Inorg. Chem.*, 2010, 1813.
31 S. Mishra, E. Jeanneau, S. Daniele and V. Mendez, *Dalton Trans.*, 2010, **39**, 7440.
32 H. Hu, M. Yu, F. Li, Z. Chen, X. Gao, L. Xiong and C. Huang, *Chem. Mater.*, 2008, **20**, 7003.
33 L. Xiong, T. Yang, Y. Yang, C. Xu and F. Li, *Biomaterials*, 2010, **31**, 7078; G. S. Yi and G. M. Chow, *Adv. Funct. Mater.*, 2006, **16**, 2324.
34 B. S. Richards and A. Shalav, *Synth. Met.*, 2005, **154**, 61; Q. H. wang and M. Bass, *Electron. Lett.*, 2004, **40**, 987; H. P. Ho, W. W. Wong and S. Y. Wu, *Opt. Eng.*, 2003, **42**, 2349.
35 Y. Bao, Q. A. N. Luu, C. Lin, J. M. Schloss, P. S. May and C. Jiang, *J. Mater. Chem.*, 2010, **20**, 8356; C. Lin, M. T. Berry, R. Anderson, S. Smith and P. S. May, *Chem. Mater.*, 2009, **21**, 3406.
36 W. Niu, S. Wu and S. Zhang, *J. Mater. Chem.*, 2010, **20**, 9113; H.-X. Mai, Y.-W. Zhang, L.-D. Sun and C.-H. Yan, *J. Phys. Chem. C*, 2007, **111**, 13721; F. Liu, E. Ma, D. Chen, Y. Yu and Y. Wang, *J. Phys. Chem. B*, 2006, **110**, 20843.
37 *CrysAlisPro*, Oxford Diffraction Ltd., Version 1.171.33.34d (release 27-02-2009 CrysAlis171 .NET) (compiled Feb 27 2009, 15 : 38 : 38).
38 B. V. Nonius, *COLLECT*, Nonius, Delft, The Netherlands (1997–2001).
39 Z. Otwinowski and W. Minor, in *Methods in Enzymology*, ed.: C. W. Carter Jr. and R. M. Sweet, Academic Press, New York, 1997, Vol. 276, p. 307.
40 R. H. Blessing, *Acta Crystallogr., Sect. A: Found. Crystallogr.*, 1995, **51**, 33.
41 R. C. Clark and J. S. Reid, *Acta Crystallogr., Sect. A: Found. Crystallogr.*, 1995, **51**, 887.
42 A. Altomare, M. C. Burla, M. Camalli, G. L. Cascarano, C. Giacovazzo, A. Guagliardi, A. G. G. Moliterni, G. Polidori and R. Spagna, *J. Appl. Crystallogr.*, 1999, **32**, 115.
43 P. W. Betteridge, J. R. Carruthers, R. I. Cooper, K. Prout and D. J. Watkin, *J. Appl. Crystallogr.*, 2003, **36**, 1487.
44 Y.-P. Du, Y.-W. Zhang, Z.-G. Yan, L.-D. Sun, S. Gao and C.-H. Yan, *Chem.–Asian J.*, 2007, **2**, 965.

